

# Collisionless Accretion onto Black Holes: Dynamics and Flares

Alisa Galishnikova,<sup>1,\*</sup> Alexander Philippov,<sup>2</sup> Eliot Quataert,<sup>1</sup> Fabio Bacchini,<sup>3,4</sup> Kyle Parfrey<sup>5</sup>,<sup>5</sup> and Bart Ripperda<sup>1,6,7</sup>

<sup>1</sup>*Department of Astrophysical Sciences, Princeton University, 4 Ivy Lane, Princeton, New Jersey 08544, USA*

<sup>2</sup>*Department of Physics, University of Maryland, College Park, Maryland 20742, USA*

<sup>3</sup>*Centre for mathematical Plasma Astrophysics, Department of Mathematics, KU Leuven, Celestijnenlaan 200B, B-3001 Leuven, Belgium*

<sup>4</sup>*Royal Belgian Institute for Space Aeronomy, Solar-Terrestrial Centre of Excellence, Ringlaan 3, 1180 Uccle, Belgium*

<sup>5</sup>*School of Mathematics, Trinity College Dublin, Dublin 2, Ireland*

<sup>6</sup>*School of Natural Sciences, Institute for Advanced Study, 1 Einstein Drive, Princeton, New Jersey 08540, USA*

<sup>7</sup>*Center for Computational Astrophysics, Flatiron Institute, 162 Fifth Avenue, New York, New York 10010, USA*



(Received 1 December 2022; accepted 15 February 2023; published 13 March 2023)

We study the accretion of collisionless plasma onto a rotating black hole from first principles using axisymmetric general-relativistic particle-in-cell simulations. We carry out a side-by-side comparison of these results to analogous general-relativistic magnetohydrodynamic simulations. Although there are many similarities in the overall flow dynamics, three key differences between the kinetic and fluid simulations are identified. Magnetic reconnection is more efficient, and rapidly accelerates a nonthermal particle population, in our kinetic approach. In addition, the plasma in the kinetic simulations develops significant departures from thermal equilibrium, including pressure anisotropy that excites kinetic-scale instabilities, and a large field-aligned heat flux near the horizon that approaches the free-streaming value. We discuss the implications of our results for modeling event-horizon scale observations of Sgr A\* and M87 by GRAVITY and the Event Horizon Telescope.

DOI: [10.1103/PhysRevLett.130.115201](https://doi.org/10.1103/PhysRevLett.130.115201)

**Introduction.**—The recent high-resolution images of synchrotron emission around the central black holes (BHs) in M87 and the Milky Way (Sgr A\*) captured by the Event Horizon Telescope (EHT) reveal asymmetric ringlike structures around the event horizon [1,2]. The radiation is produced by relativistic plasma on event-horizon scales. General-relativistic magnetohydrodynamic (GRMHD) simulations are a conventional tool for modeling accretion onto BHs [3]. In conjunction with GR radiative transfer, one can predict aspects of the observed radiation, including spatially resolved images, from these numerical models [4]. This theoretical framework allows for a direct comparison of GRMHD simulations and observations. However, the accreting plasma in these systems is collisionless, which makes the simplifying assumptions of GRMHD approach formally inapplicable. Theoretical models thus require a kinetic approach, which describes collisionless plasmas from first principles. In this Letter, we present global GR kinetic simulations of BH accretion and determine the ways in which they differ from conventional fluid models.

Supermassive BHs show emission across the electromagnetic spectrum. Besides a relatively constant background emission, Sgr A\* also exhibits episodic bright flares in the near-infrared and x rays (e.g., [5–7]). The observed power-law emission implies a presence of accelerated particles (electrons and possibly positrons) near the BH. Studying the generation of nonthermal particles is not

possible within GRMHD fluid models and requires a kinetic approach. Additionally, GRMHD approach does not accurately capture reconnection of magnetic field lines, which is conjectured to be responsible for particle energization and flares [6,8–12]. Specifically, the rate of reconnection, which regulates the energization efficiency and can be responsible for the duration of flares [13], is known to be substantially faster in collisionless plasma (e.g., [14–16]). Ideal GRMHD approach also assumes an isotropic Maxwellian plasma distribution function, while collisionless plasmas easily develop pressure anisotropy along and across the magnetic field direction [17,18], which leads to the development of plasma instabilities. The saturation of these instabilities and a possible large field-aligned heat flux regulate the thermodynamic state of the plasma, potentially affecting the global accretion dynamics and its observational properties.

**Methods.**—In order to study accretion of collisionless plasmas onto BHs, we perform kinetic simulations using the GR particle-in-cell (GRPIC) code ZELTRON which solves Maxwell's equations and the equations of motion for individual macroparticles in the 3 + 1 formalism [19]. We also study the same problem with identical initial conditions using the GRMHD code ATHENA++ [20], which allows for a side-by-side comparison of the two approaches. Both approaches utilize horizon-penetrating Kerr-Schild coordinates. We measure distance in units of the gravitational radius,  $r_g = GM/c^2$ , where  $G$  is the

gravitational constant,  $M$  is the mass of the BH, and  $c$  is the speed of light; time is measured in light crossing times of the gravitational radius,  $r_g/c$ .

In GRPIC method, the substantially reduced ion-to-electron mass ratio,  $m_i/m_e$ , allows us to resolve all microphysical plasma scales and respect the correct hierarchy of scales [21], i.e., all plasma scales are significantly smaller than  $r_g$ . Because of their high computational cost, our simulations are limited to two-dimensional, axisymmetric accretion onto a BH in the  $r$ - $\theta$  plane, which is aligned with the BH spin,  $a = 0.95$ . Since there is no kinetic equilibrium solution known for this problem [22], and motivated by the relevance to the accretion flow onto Sgr A\* [23], we start with a zero-angular-momentum spherically symmetric distribution of stationary plasma. Previous work shows that this accretion problem behaves similarly in many respects to one incorporating rotating initial conditions [24]. Specifically, this accretion problem leads to a magnetically arrested flow on event-horizon scales with a similar jet power and similar magnetic flux eruptions as in rotating models; in addition, frame dragging by the spinning BH and magnetic torques are enough to produce significant angular momentum in the inner  $\sim 10$ – $20r_g$ , similar to that found in simulations with rotating torus initial conditions [25]. We set an initially constant density, pressure, and magnetic field aligned with the spin axis throughout the box, and add randomly distributed magnetic loops [26] to mimic turbulence expected in accretion disks.

We initialize a thermal plasma with  $k_B T_{inj} \approx 0.02 m_i c^2$ , which corresponds to a Bondi radius  $r_B = 2GM/c_s^2 \approx 50r_g$ , where  $k_B$  is the Boltzmann constant and  $c_s$  is the sound speed. We focus on two initial values of the plasma- $\beta$  parameter,  $\beta_0 = P/P_{B_0} = 4$  or  $10$ , where  $P$  is the gas pressure and  $P_{B_0}$  is the magnetic pressure of the initial vertical magnetic field  $B_0$ . Our GRPIC simulations use mass ratios of  $m_i/m_e = 1$  and  $3$ ; the thermal Larmor radius of ions is set to be  $\rho_L = v_{th} m_i c / e B_0 = 0.018 r_g$ . Below we show results of simulations with mass ratio  $m_i/m_e = 1$ , which we are able to run until  $1000r_g/c$ . The dynamics of ions in simulations with  $m_i/m_e = 3$  until  $100r_g/c$  is similar compared to the case with  $m_i/m_e = 1$  [26].

Our simulation domain extends from the inner boundary, located below the event horizon, to the outer boundary at  $100r_g$ . We employ constant boundary conditions at the outer boundary in GRMHD simulations and use absorbing boundary conditions supplemented with injection of fresh plasma in GRPIC simulations [26]. In highly magnetized regions plasma density can get depleted; we therefore apply a ceiling value for the magnetization parameter  $\sigma = B^2/[4\pi n(m_e + m_i)c^2] \approx 30$  in both approaches. In GRPIC simulations, we add electron-positron pairs when  $\sigma$  is above this threshold, thus mimicking a pair cascade expected in these regions [27–30].

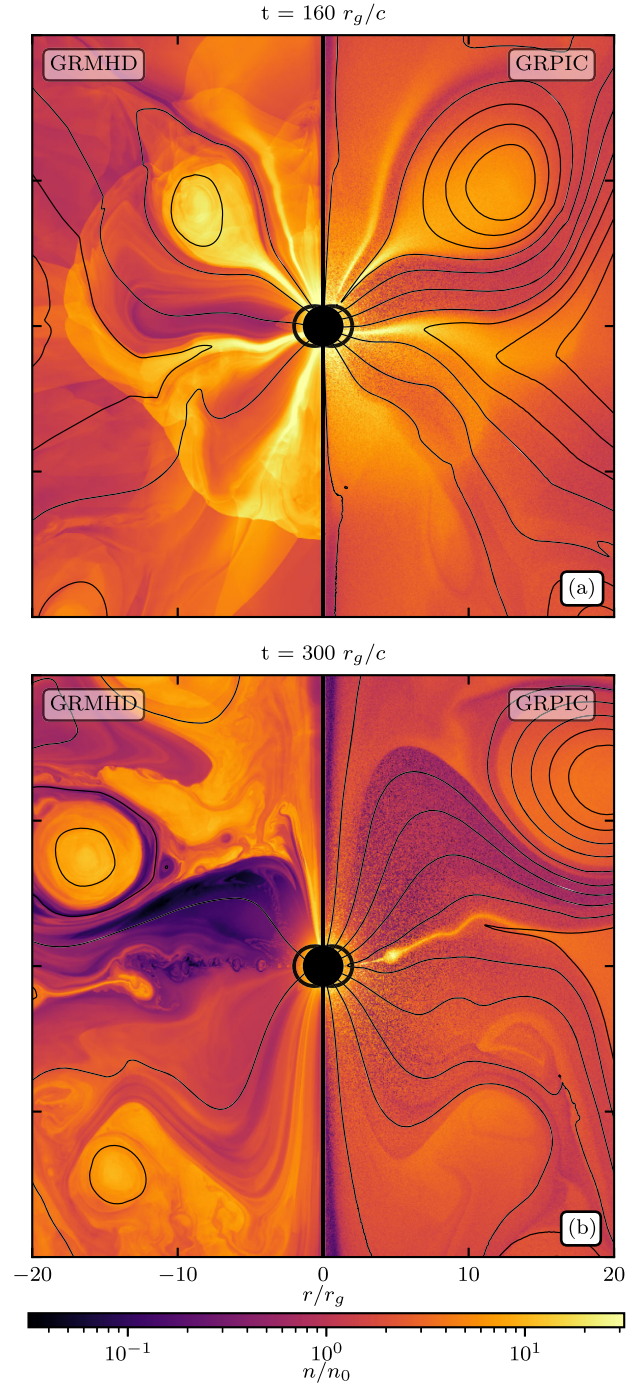


FIG. 1. Comparison of fluid and kinetic simulations of accretion onto a rotating BH. The color shows  $n/n_0$ , which corresponds to the plasma number density in GRMHD simulations (left) and ion and positron number density in GRPIC simulations (right) in a region close to the BH ( $20r_g$ ). The region inside the BH event horizon,  $r_h = r_g(1 + \sqrt{1 - a^2})$ , is shown by a black circle. Thin black lines represent the magnetic field lines, a thick black line outlines the ergosphere. The same quantities are shown at a time of  $160r_g/c$  (a) and  $300r_g/c$  (b). Several current sheets form and reconnect (a), leading to a flaring state (b).

**Results.**—In Fig. 1 we show a side-by-side comparison of the evolution of the number density  $n$  of the accreting plasma in GRMHD (plasma number density, left) and GRPIC (ion and positron number density, right) simulations with  $\beta_0 = 4$  at a time of  $160r_g/c$  (a) and  $300r_g/c$  (b);  $n_0$  corresponds to the initial value. Both panels show a zoom into the inner  $20r_g$ . Initially, the accreting plasma is free-falling onto the BH within the Bondi radius, dragging the magnetic field lines towards the event horizon (a). Inflow streams with a similar structure in both GRPIC and GRMHD simulations are formed: a thin inflow is formed just below the equator, and a squeezed large loop is accreting above the equator. As the accretion proceeds, the BH's rotation and magnetic flux on the event horizon, which becomes dynamically important, lead to the launching of magnetically dominated outflows. The accretion stalls when the magnetic field becomes too strong, leading to thinning of the inflow streams into current sheets, onset of reconnection (b) [11,12], and the evacuation of the accretion flow in the equatorial plane (eruption). Eventually, the magnetic loop above the equator evacuates as an outflowing density bubble. Since the rate of collisionless reconnection is faster by a factor of a few, compared to MHD, the two numerical results ultimately diverge.

The reconnection physics manifests itself in the time evolution of the accretion rate,  $\dot{M} = -\int_{\theta} \int_{\phi} \sqrt{-g} \rho u^r d\theta d\phi$ , and magnetic flux on the horizon,  $\Phi = 0.5 \int_{\theta} \int_{\phi} \sqrt{-g} \times |B^r| d\theta d\phi$ , shown in Figs. 2(a) and 2(b), which we normalize by the Bondi accretion rate,  $\dot{M}_B$ , and initial value of the magnetic flux on the horizon,  $\Phi_0$ . Here,  $g$  is the metric determinant, and  $u^\mu$  is the fluid four-velocity. Initially, the infalling plasma in both approaches causes an increase in  $\dot{M}/\dot{M}_B$  and  $\Phi/\Phi_0$  at a similar rate, reaching saturation in the magnetically arrested state [31]. GRMHD simulation shows two  $\dot{M}$  maxima followed by postaccretion eruption events associated with the onset of the decline of  $\Phi$  at  $\approx 200$  and  $600r_g/c$ . The GRPIC simulation, however, shows one  $\dot{M}$  maximum followed by an eruption event at  $\approx 380r_g/c$  and another accretion period starting at  $\approx 800r_g/c$ . Therefore, even though reconnection is more efficient, the variability—the frequency of the eruption events—*might be* smaller in the kinetic approach, as the accretion stalls due to its regulation by the efficient large-scale reconnection. Consequently, both  $\dot{M}/\dot{M}_B$  and  $\Phi/\Phi_0$  saturate at smaller values over a longer time period in GRPIC simulation.

A comparison of the two approaches due to the reconnection physics alone is demonstrated by simulations with an initially vertical uniform magnetic field [no loops, in Figs. 2(a) and 2(b)]. Here, since kinetic reconnection is more efficient, GRPIC simulation shows a steeper exponential decline in  $\Phi/\Phi_0$  compared to GRMHD approach [13].

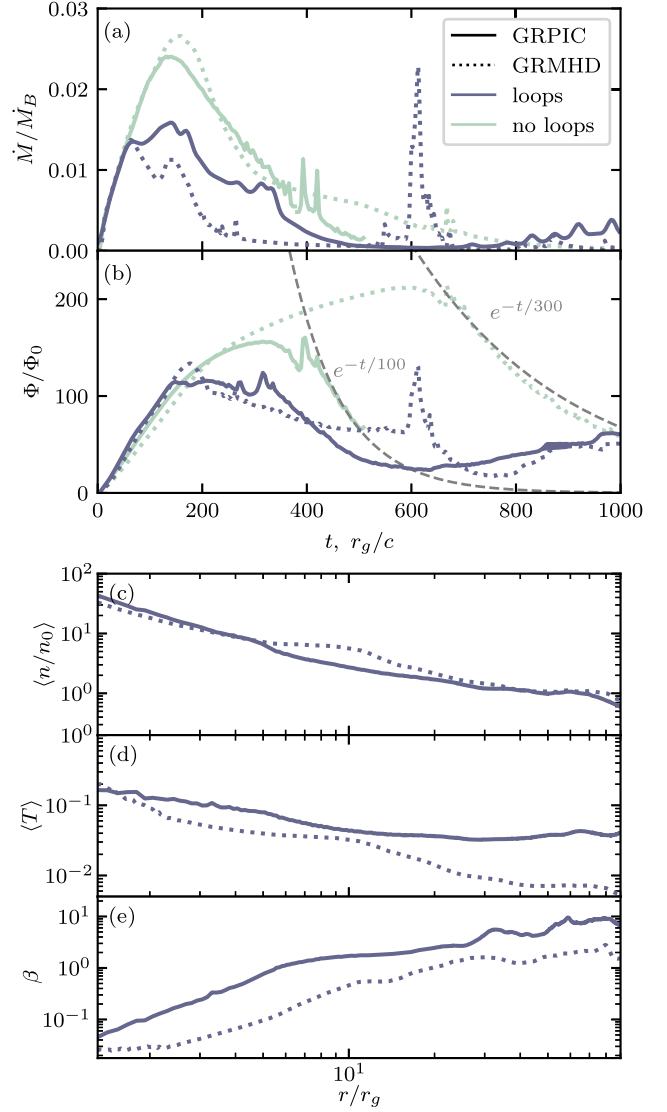


FIG. 2. Evolution of averaged quantities in GRPIC (solid lines) and GRMHD (dotted) simulations. (a) Time evolution of the accretion rate in units of the Bondi accretion rate,  $\dot{M}/\dot{M}_B$ ; (b) magnetic flux on the horizon normalized by its initial value  $\Phi/\Phi_0$ . The gray dashed lines give the exponential fit for the decay rate of  $\Phi/\Phi_0$ , highlighting the difference of the reconnection rate. (c) Mean profiles of number density,  $\langle n/n_0 \rangle$ ; (d) temperature,  $\langle T \rangle$ , and (e) plasma- $\beta = \langle P \rangle / \langle P_B \rangle$ , as a function of radius  $r/r_g$ , averaged over  $t = [100 - 200]r_g/c$ . The runs initialized with the turbulent magnetic field are shown by a darker color (loops), with a vertical uniform magnetic field—a lighter color (no loops).

We show radial profiles (integrated over  $\theta$  during the first accretion event,  $100-200r_g/c$ ) of density  $\langle n/n_0 \rangle$  (c), temperature  $\langle T \rangle$  (d), and  $\beta = \langle P \rangle / \langle P_B \rangle$  (e) [26]. We find a striking similarity of the number density profiles, while the temperature and  $\beta$  profiles show a significant difference between the two approaches due to the nonideal physics described next.



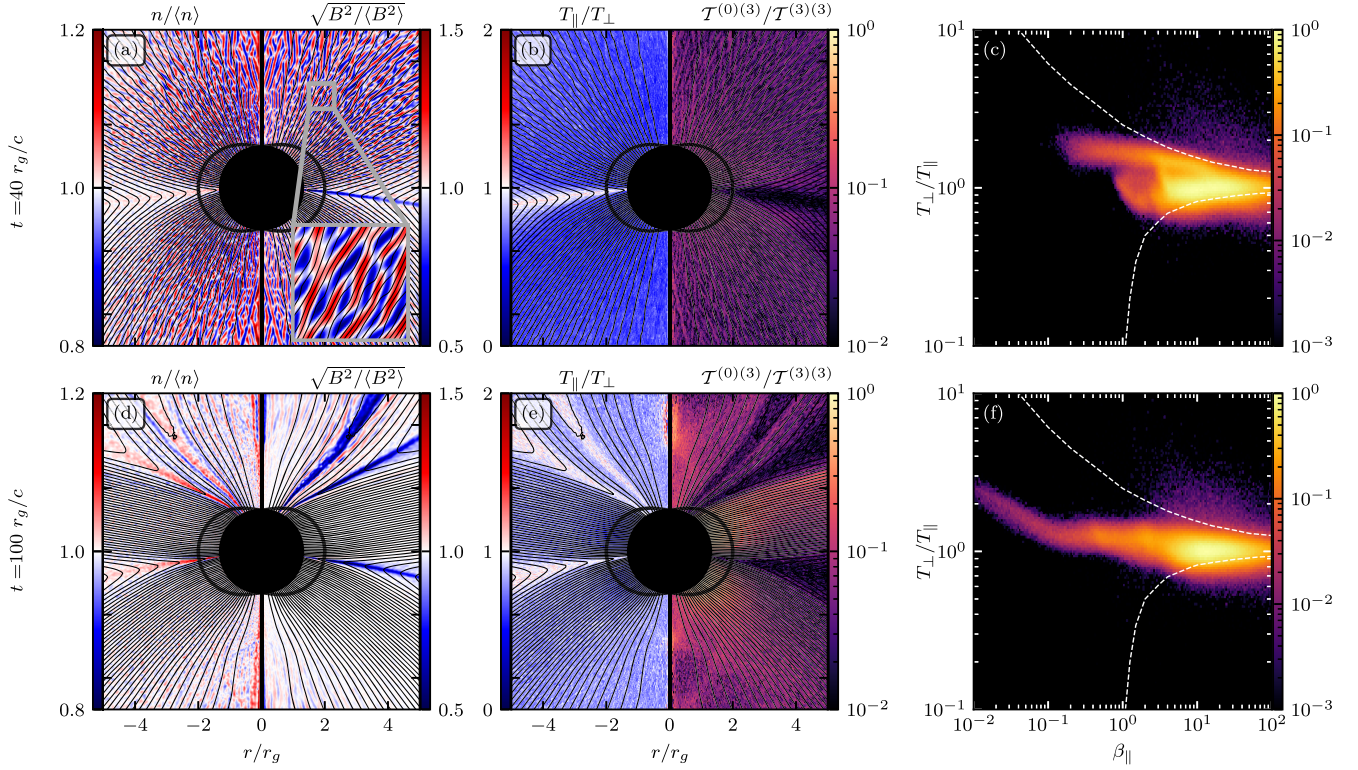


FIG. 3. Anisotropy and heat flux in GRPIC simulation initialized with  $\beta_0 = 10$ . Each row corresponds to a different moment in time:  $40r_g/c$  (a)–(c), and  $100r_g/c$  (d)–(f). First column: number density (left) and magnetic field (right) fluctuations. Second column: temperature anisotropy  $T_{\parallel}/T_{\perp}$  (left) and the ratio of nonideal and ideal matter stress-energy tensor components in the tetrad frame  $\mathcal{T}^{(0)(3)}/\mathcal{T}^{(3)(3)}$ , which represents the ratio of parallel heat flux  $q_{\parallel}$  and parallel pressure  $P_{\parallel}$ . The black circle and black lines represent the event horizon, ergosphere, and magnetic field lines as in Fig. 1. Third column: probability density as a function of  $\beta_{\parallel} = P_{\parallel}/P_B$  and temperature anisotropy  $T_{\perp}/T_{\parallel}$ . White dashed lines correspond to the boundaries of the growth rate of mirror (top) and firehose (bottom) instabilities exceeding 10% of the ion cyclotron frequency calculated using [33]. A mirror instability develops and saturates at  $40r_g/c$ , for which we show a zoom into the structure of the instability (a).

To quantify another key feature of the kinetic approach, departure of the accreting plasma from thermal equilibrium, we calculate the matter stress-energy tensor in GRPIC simulation,  $\mathcal{T}^{\mu\nu}_{\text{matter}}$ , which can be used to derive the pressure tensor,  $P^{\mu\nu}$ , and the heat flux,  $q^{\mu}$ . We project these quantities onto a tetrad,  $e^{\mu}_{(\nu)}$ , where  $e^{\mu}_{(0)}$  is directed along the (Eckart) fluid velocity and  $e^{\mu}_{(3)}$  is along the magnetic field in the fluid frame. The pressure tensor in this tetrad frame is diagonal,  $\text{diag}(P_{\perp}, P_{\perp}, P_{\parallel})$ , where parallel and perpendicular components are measured with respect to the magnetic field direction in the fluid frame.

Ion quantities from a GRPIC simulation initialized with  $\beta_0 = 10$  are shown in Fig. 3, where the two rows correspond to times of  $40r_g/c$  and  $100r_g/c$ . The first column shows number density  $n/\langle n \rangle$  (left) and magnetic field  $\sqrt{B^2/\langle B^2 \rangle}$  (right) fluctuations; second—temperature anisotropy  $T_{\parallel}/T_{\perp}$  (left) and ratio of the two stress-energy tensor components  $\mathcal{T}^{(0)(3)}/\mathcal{T}^{(3)(3)}$  in the tetrad frame (right), where  $\mathcal{T}^{(0)(3)}$  corresponds to parallel heat flux  $q_{\parallel}$  (absent in ideal GRMHD approach). The last column

shows an ion probability density plotted as a function of  $\beta_{\parallel} = P_{\parallel}/P_B$  and  $T_{\perp}/T_{\parallel}$ . The polar inflow of the plasma leads to the build up of magnetic field, and an associated increase in  $P_{\perp} \propto B$ . The deviation from thermal equilibrium with  $T_{\perp} > T_{\parallel}$  leads to the excitation of small-scale plasma density and magnetic field fluctuations (a), where we also show a zoom into a small region. This is a kinetic-scale mirror instability which develops when plasma crosses a  $\beta$ -dependent temperature anisotropy threshold, as shown in (c). The saturated strength of the magnetic field fluctuations,  $|1 - \sqrt{B^2/\langle B^2 \rangle}|$ , is of order of a few tens of percent, consistent with local simulations [17,18,32]. At earlier times in the simulation, transiently, we observe the development of the electromagnetic firehose instability in the equatorial region, where  $T_{\parallel} > T_{\perp}$  [26].

At early times (b), the effective collisions due to particle scattering by the kinetic-scale fluctuations lead to a suppression of the heat flux,  $\mathcal{T}^{(0)(3)} \approx 0.1\mathcal{T}^{(3)(3)}$ . We find that  $q_{\parallel}$  is also  $\approx 0.1$  of the value corresponding to the free streaming of particles along magnetic field lines [26]. As the accretion proceeds and the value of  $\beta$  near the event

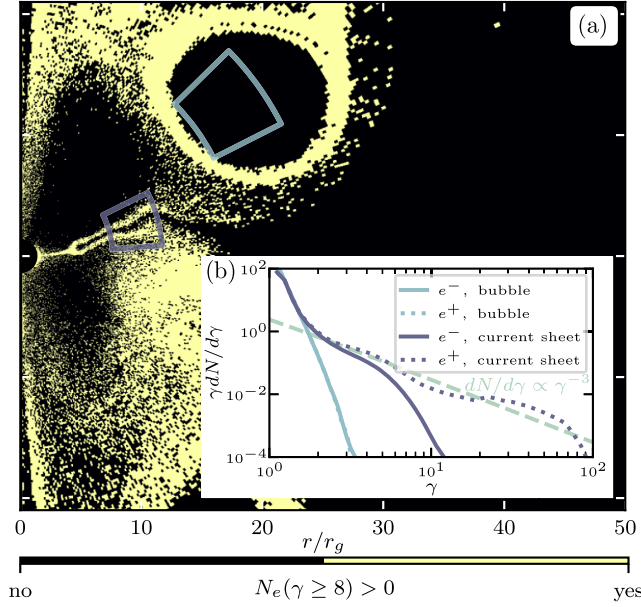


FIG. 4. Panel (a) shows the presence (yes or no) of energetic electrons with  $\gamma \geq 8$  throughout the GRPIC simulation at  $300r_g/c$  [shown in Fig. 1(b), right]. To avoid low density regions near the axis, we show regions above the density threshold,  $n > n_0/2$ . Panel (b) shows particle spectra measured inside the outflowing bubble (blue) and in the current sheet (purple), which are outlined in (a) by the respective colors.

horizon drops below 1, the inflow is no longer accompanied by significant density or magnetic field fluctuations (d), which is consistent with the plasma being pushed away from the pressure-anisotropy instability boundaries (f). The absence of scattering on microscale magnetic field fluctuations leads to larger values of the nonideal components of the stress-energy tensor,  $\mathcal{T}^{(0)(3)}/\mathcal{T}^{(3)(3)} \approx 1$ , outside of the current sheets (e), and  $q_{\parallel}$  also approaches the free-streaming value. These nonideal effects contribute to substantial differences between GRPIC and GRMHD temperature profiles [Fig. 2(d)].

To understand where particles are accelerated, we highlight regions with highly energetic particles with a Lorentz factor  $\gamma \geq 8$  in GRPIC simulation at  $300r_g/c$  in Fig. 4 [the same time snapshot as Fig. 1(b), right]. These particles are predominantly located around the current sheets and the outflowing dense bubble. We measure particle spectra (b) in the regions outlined by corresponding colored wedges in (a). The spectral slope of  $\approx -3$  (current sheet) is consistent with particle acceleration in relativistic magnetic reconnection for the measured magnetization parameter  $\sigma \approx 5$  in the upstream [14,34,35]. As  $\sigma$  increases due to evacuation of plasma in the jet region, we find a harder slope of  $\approx -2$ , consistent with higher  $\sigma \gtrsim 10$  around the current sheet. Positively charged particles are accelerated more efficiently [Fig. 4(b)] because their acceleration by the electric fields inside the current sheet is aligned with the direction of the outflow motion above it [36].

*Discussion.*—A fully kinetic approach is crucial for understanding the dynamics of plasmas accreting onto supermassive BHs such as Sgr A\* and M87\*. Using global GRPIC simulations of accretion onto a rotating BH, we highlight three significant differences relative to matched GRMHD simulations: (1) differences in the physics of magnetic reconnection can, in principle, change the frequency of eruption episodes in GRPIC relative to GRMHD approach; (2) GRPIC method includes pressure anisotropy with respect to the magnetic field and the associated kinetic instabilities; (3) in GRPIC method a large field-aligned heat flux near the horizon is important in regulating the plasma temperature. Our kinetic approach allows for self-consistent modeling of particle acceleration during flaring episodes powered by magnetic reconnection, which opens up a unique opportunity for comparing theory with observed radiation spectra and light curves. Studying the relative heating and acceleration of ions and electrons will require a more realistic ion-to-electron mass ratio, which we currently lack in our simulations. In conjunction with GR radiative transfer, extension of our simulations to a larger mass ratio and 3D will allow us to compare spatially resolved images, polarization maps, and lightcurves constructed from GRPIC simulations to GRAVITY and EHT data. Future GRPIC simulations will rigorously measure the nonideal corrections to the GRMHD stress tensor for a range of plasma conditions, which can then be included in GRMHD simulations [37,38] to improve their realism.

This work was supported by NASA Grant No. 80NSSC22K1054 and NSF Grant No. PHY-2231698. E. Q. and A. G. were supported in part by a Simons Investigator Grant from the Simons Foundation. Computing resources were provided and supported by Princeton Institute for Computational Science and Engineering; and by the VSC (Flemish Supercomputer Center), funded by the Research Foundation Flanders (FWO) and the Flemish Government—department EWI. This research is part of the Frontera computing project at the Texas Advanced Computing Center (LRAC-AST21006). Frontera is made possible by NSF Award OAC-1818253. F. B. acknowledges support from the FED-TWIN programme (profile Prf-2020-004, project “ENERGY”) issued by BELSPO. Support for this work was provided by NASA through the NASA Hubble Fellowship Grant No. HST-HF2-51518.001-A awarded by the Space Telescope Science Institute, which is operated by the Association of Universities for Research in Astronomy, Incorporated, under NASA Contract No. NAS5-26555. This research was facilitated by Multimessenger Plasma Physics Center (MPPC), NSF Grant No. PHY-2206607.

\*alisag@princeton.edu

- [1] Event Horizon Telescope Collaboration, *Astrophys. J. Lett.* **875**, L1 (2019).
- [2] Event Horizon Telescope Collaboration, *Astrophys. J. Lett.* **930**, L12 (2022).
- [3] O. Porth, K. Chatterjee, R. Narayan *et al.*, *Astrophys. J. Suppl. Ser.* **243**, 26 (2019).
- [4] R. Gold, A. E. Broderick, Z. Younsi *et al.*, *Astrophys. J.* **897**, 148 (2020).
- [5] GRAVITY Collaboration, *Astron. Astrophys.* **618**, L10 (2018).
- [6] K. Dodds-Eden, D. Porquet, G. Trap *et al.*, *Astrophys. J.* **698**, 676 (2009).
- [7] F. Yusef-Zadeh, H. Bushouse, M. Wardle *et al.*, *Astrophys. J.* **706**, 348 (2009).
- [8] S. Markoff, *Astrophys. J.* **618**, L103 (2005).
- [9] A. E. Broderick and A. Loeb, *Mon. Not. R. Astron. Soc.* **367**, 905 (2006).
- [10] J. Dexter, A. Tchekhovskoy, A. Jimnez-Rosales *et al.*, *Mon. Not. R. Astron. Soc.* **497**, 4999 (2020).
- [11] B. Ripperda, F. Bacchini, and A. A. Philippov, *Astrophys. J.* **900**, 100 (2020).
- [12] B. Ripperda, M. Liska, K. Chatterjee *et al.*, *Astrophys. J. Lett.* **924**, L23 (2022).
- [13] A. Bransgrove, B. Ripperda, and A. Philippov, *Phys. Rev. Lett.* **127**, 055101 (2021).
- [14] L. Sironi and A. Spitkovsky, *Astrophys. J. Lett.* **783**, L21 (2014).
- [15] A. Bhattacharjee, Y. Huang, H. Yang, and B. Rogers, *Phys. Plasmas* **16**, 112102 (2009).
- [16] Fast reconnection (i.e., proceeding at a rate independent of the Lundquist number for collisional fluids, or the ratio between the current sheet length and plasma skin depth for collisionless plasmas) can be realized in both MHD and PIC, but its rate in MHD is substantially smaller (by a factor of 10) than the corresponding reconnection rate in kinetic simulations.
- [17] M. W. Kunz, A. A. Schekochihin, and J. M. Stone *Phys. Rev. Lett.* **112**, 205003 (2014).
- [18] M. A. Riquelme, E. Quataert, and D. Verscharen, *Astrophys. J.* **800**, 27 (2015).
- [19] K. Parfrey, A. Philippov, and B. Cerutti, *Phys. Rev. Lett.* **122**, 035101 (2019).
- [20] C. J. White, J. M. Stone, and C. F. Gammie, *Astrophys. J. Suppl. Ser.* **225**, 22 (2016).
- [21] The real scale separation between the kinetic scales and  $r_g$  or the size of the system can be up to 10 or 20 orders of magnitude respectively, which is unachievable with numerical simulations. Current GRPIC simulations are also incapable of reproducing the realistic scale separation between ions and electrons.
- [22] In a collisionless plasma of a small Larmor radius, initial conditions such as a rotating torus are out-of-equilibrium along the magnetic field lines. As is mentioned in the text, fully kinetic global equilibria are currently not known.
- [23] E. Quataert, *Astron. Nachr. Suppl.* **324**, 435 (2003).
- [24] S. M. Ressler, C. J. White, E. Quataert, and J. M. Stone, *Astrophys. J. Lett.* **896**, L6 (2020).
- [25] The primary difference between these two accretion problems is in the jet properties far from the BH [24], which is not a focus of this Letter.
- [26] See Supplemental Material at <http://link.aps.org/supplemental/10.1103/PhysRevLett.130.115201> for additional discussion of the numerical setup of GRPIC and GRMHD simulations, measurement of the pressure anisotropy in the GRPIC simulation with  $m_i/m_e = 3$ , and details about the calculation of the plasma stress-energy tensor, pressure tensor, and heat flux.
- [27] V. S. Beskin, Y. N. Istomin, and V. I. Pavlov, *Sov. Astron.* **36**, 642 (1992), <https://ui.adsabs.harvard.edu/abs/1992SvA...36..642B/abstract>.
- [28] K. Hirokuni and I. Okamoto, *Astrophys. J.* **497**, 563 (1998).
- [29] B. Crinquand, B. Cerutti, A. Philippov, K. Parfrey, and G. Dubus, *Phys. Rev. Lett.* **124**, 145101 (2020).
- [30] A. Y. Chen and Y. Yuan, *Astrophys. J.* **895**, 121 (2020).
- [31] A. Tchekhovskoy, R. Narayan, and J. C. McKinney, *Mon. Not. R. Astron. Soc.* **418**, L79 (2011).
- [32] In principle, a pair plasma at moderate  $\beta$  is unstable to the ion-cyclotron instability at lower values of the pressure anisotropy. However, we observe the mirror instability to dominate in the saturated phase, in agreement with local simulations [18].
- [33] D. Verscharen and B. D. G. Chandran, *Res. Notes AAS* **2**, 13 (2018).
- [34] F. Guo, H. Li, W. Daughton, and Y. H. Liu, *Phys. Rev. Lett.* **113**, 155005 (2014).
- [35] G. R. Werner, D. A. Uzdensky, B. Cerutti *et al.*, *Astrophys. J. Lett.* **816**, L8 (2016).
- [36] B. Cerutti, A. Philippov, K. Parfrey, and A. Spitkovsky, *Mon. Not. R. Astron. Soc.* **448**, 606 (2015).
- [37] M. Chandra, C. F. Gammie, F. Foucart, and E. Quataert, *Am. Astron. Soc.* **810**, 162 (2015).
- [38] F. Foucart, M. Chandra, C. F. Gammie *et al.*, *Mon. Not. R. Astron. Soc.* **470**, 2240 (2017).